JCTC Journal of Chemical Theory and Computation

Revised Implicit Solvent Model for the Simulation of Surfactants in Aqueous Solutions. 2. Modeling of Charged Headgroups at Oil−Water Interface

Shintaro Morisada,† Hiroyuki Shinto,* and Ko Higashitani

Department of Chemical Engineering, Kyoto University, Nishikyo-ku, Kyoto 615-8510, Japan

Received October 23, 2006

Abstract: The revised implicit solvent model (ISM-2) for the simulation of cationic surfactants in water was proposed in the previous study (*J. Phys. Chem. B* **2005**, 109, 11762): no water molecules of the solvent are explicitly treated, and their effects are incorporated using the solvent-averaged interactions between the surfactant segments in water, where the interactions between the hydrocarbon sites of the surfactants are allowed to vary depending on their surroundings. In the present study, the representation of a charged headgroup at the liquid−liquid interface between the hydrocarbon oil and the implicit water has been improved, where the free energy change due to the transfer of the charged headgroup across the interface is taken into account. The present model (ISM-3) has been applied to the molecular dynamics simulations of (i) the single preformed micelle of 30 *n*-decyltrimethylammonium chloride (C_{10}TAC) cationic surfactants in water and (ii) 343 C_{10}TAC surfactants uniformly dispersed in water, where the corresponding systems are also simulated using the ISM-2 for comparison. The first simulations showed that the ISM-3 as well as the ISM-2 is applicable to the simulation of the preformed micelle of the average aggregate size for C_{10}TAC. The second simulations demonstrated that the ISM-3 can represent the surfactant self-assembling plausibly, while the ISM-2 fails to do so because of the rude treatment of the charged headgroups at the interface. The results will be compared with those from experiments and atomistic model simulations.

1. Introduction

Shape, stability, and average size of surfactant aggregates in solutions have been of great interest for researchers and engineers in many fields. The surfactant aggregates have been investigated at the molecular level using the molecular dynamics (MD) and the Monte Carlo (MC) simulations,[1−13] which are popular tools for atomistic description of matter and materials.[14−16] However, the quantitative simulation of the surfactants in a solution computationally costs too much, because a huge number of the solvent molecules must be treated besides the solute molecules of interest. If the solvent molecules can be treated implicitly, the computational cost is drastically reduced, which makes the quantitative simulations of surfactant solutions more accessible to the researchers and the engineers. Such implicit treatment of the solvent is referred to as an implicit solvent model (ISM),[17] where the effects of the solvent are incorporated into the interactions between the solutes. When the concentration of the solutes is not very high, the effective interactions between them are plausibly represented by the potential of mean force (PMF), which is the solvent-averaged free energy as a function of the configuration of the solutes.

In our previous study,[18] the ISM was proposed for the simulation of cationic surfactants in water, where the effective interactions between the surfactant segments are given by assuming the site−site pair additivity of the PMFs

* Corresponding author phone: +81-75-383-2672; fax: +81-75-383-2652; e-mail: shinto@cheme.kyoto-u.ac.jp.

† Present address: Department of Environmental Chemistry and Engineering, Tokyo Institute of Technology, Nagatsuta, Midori-ku, Yokohama 226-8502, Japan.

10.1021/ct600311t CCC: $37.00
Published on Web 03/24/2007

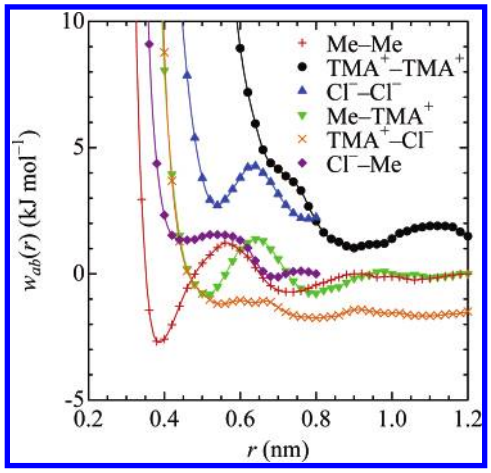

Figure 1. Potentials of mean force for solute pairs in ambient water at infinite dilution. The solid lines are the guides for the eyes.

in water at infinite dilution. The ISM was then revised to represent the hydrocarbon interior of the surfactant aggregates more appropriately: in this revised model (ISM-2), the interactions between the hydrophobic sites of the surfactants are varied depending on their surroundings, namely, the local hydrocarbon density.[19] It is noted that Lazaridis et al.[20] also reported similar implicit solvent simulations of the zwitterionic surfactants.

Using the ISM-2, we have simulated the self-assembly of the cationic surfactants in water to encounter the strange result, as will be seen in section 3.2: only a few aggregates became large, and the other surfactants remained as monomers or small aggregates, where the large aggregates often included the charged headgroups of the surfactants in the hydrocarbon interior. This result is considered to be implausible because the charged headgroups should exist in water more favorably than in the hydrocarbon interior. The aim of the present study is to improve the ISM-2 by correcting the representation of the charged headgroups.

In this paper, we improve the representation of a charged headgroup at the liquid−liquid interface between the hydrocarbon oil and the implicit water, where the free energy change due to the transfer of the charged headgroup across the interface is taken into account. This model (ISM-3) is applied to the MD simulations of the aqueous surfactant solutions starting from two types of initial configurations: (i) a single preformed micelle of the surfactants in water and (ii) the surfactant monomers uniformly dispersed in water. To clarify the effect of the revision in the ISM-3, the simulation results are compared with those from the ISM-2.

2. Simulation Methods

2.1. Implicit Solvent Models. We consider *n*-decyltrimethylammonium chloride [$CH_3(CH_2)_9$-$N(CH_3)_3^+Cl^-$ or C_{10}TAC] and water as a cationic surfactant and a solvent, respectively. To construct the force field for the surfactant molecule in water using the PMFs, the following technique was employed. The hydrophilic and the hydrophobic groups of the surfactant were approximated by a tetramethylammonium ion [$(CH_3)_4N^+$ or TMA^+] and a chain of methane molecules (CH_4 or Me), respectively.[18,19] Figure 1 shows the PMFs $w_{ab}(r)$ for 6 different binary combinations with Me, TMA^+, and Cl^- in ambient water at infinite dilution, which were computed using the atomistic model MD simulations in our previous studies.[21] The surfactant of $CH_3(CH_2)_9$-$N(CH_3)_3^+Cl^-$ was mimicked as $(Me)_{10}$-TMA^+Cl^-, that is, $t_{10}h^+Cl^-$, where t and h^+ denote the hydrophobic and the hydrophilic sites, respectively.

Table 1. Molecular Geometry of $t_{10}h^+$ Surfactant

	bond length (nm)	bond angle (deg.)
t-t	0.153	
t-h^+	0.280	
t-t-t		109.5
t-t-h^+		126.4

2.1.1. Previous Model (ISM-2).[19] All the intermolecular interactions were given by assuming the site−site pair additivity of the PMFs, except for the interaction between the hydrophobic sites (see eq 3). The PMFs for separations beyond the range of the computed PMFs (i.e., $r > 0.8$ or 1.2 nm) were given by

$$w_{ab}(r) = \frac{1}{4\pi\epsilon_r^{\,w}\epsilon_0}\frac{Q_aQ_b}{r} \tag{1}$$

where Q_a is the point charge of site a, ϵ_0 is the permittivity of the vacuum, and $\epsilon_r^{\,w}$ is the relative permittivity of water; the experimental value of $\epsilon_r^{\,w} = 77.6$ at $T = 300$ K was used.[22]

As for the intramolecular interactions of the $t_{10}h^+$ surfactant, the PMF between the t and the h^+ sites (see Figure 1) and the corrected PMF between the t sites (see eq 3) were included, only when these sites were separated at least four bonds. The bond lengths and the bond angles were fixed at constant values, as listed in Table 1. The torsional potential of Ryckaert and Bellemans[23] was used for t-t-t-t and t-t-t-h^+

$$u_{\text{torsion}}(\phi) = \sum_{n=0}^{5} k_n \cos^n\phi \tag{2a}$$

$$\left.\begin{aligned} k_0 &= +1.541 \times 10^{-20}\text{J} \\ k_1 &= +2.019 \times 10^{-20}\text{J} \\ k_2 &= -2.179 \times 10^{-20}\text{J} \\ k_3 &= -0.508 \times 10^{-20}\text{J} \\ k_4 &= +4.357 \times 10^{-20}\text{J} \\ k_5 &= -5.230 \times 10^{-20}\text{J} \end{aligned}\right\} \tag{2b}$$

where ϕ is the dihedral angle, and $\phi = 0$ corresponds to the trans conformation.

The ISM family[18,19] is based on the PMFs composed of the direct and the solvent-induced interactions. However, the solvent-induced interactions between the hydrophobic sites are negligible in the interior of the surfactant aggregates such as micelles, because water molecules hardly exist there. The interaction force between the hydrophobic sites, f_{tt}, was then represented by the PMF and the Lennard-Jones (LJ) terms

$$f_{tt} = -(1 - \alpha_{ia,jb})\cdot\frac{dw_{MeMe}(r)}{dr} - \alpha_{ia,jb}\cdot\frac{du_{LJ}(r)}{dr} \tag{3a}$$

$$u_{LJ}(r) = 4\epsilon_t\left[\left(\frac{\sigma_t}{r}\right)^{12} - \left(\frac{\sigma_t}{r}\right)^{6}\right] \quad (3b)$$

where $w_{MeMe}(r)$ is the PMF for the Me−Me pair in Figure 1, $\epsilon_t = 0.994 \times 10^{-21}$ J, and $\sigma_t = 0.3923$ nm; the latter two are the energy and the size parameters of the LJ potential for *n*-alkane, respectively.[23] The distribution parameter $\alpha_{ia,jb}$ is allowed to vary from 0 to 1, depending on the local packing ratio of the hydrocarbon sites around sites *a* and *b* of interest.

To define the local packing ratio of the hydrocarbon around the hydrophobic site *a* on molecule *i*, Γ^t_{ia}, we regarded every hydrophobic site as a sphere of radius $\sigma_t/2$ and then computed the portion that the spherical shell of inner radius $\sigma_t/2$ and outer radius σ_t around site *a* cuts out from the spheres of all the other sites, as illustrated in Figure 2. The spherical shell around site *a* on molecule *i* cuts out from the sphere of site *b* on molecule *j*, the shaded portion, whose volume $V^t_{ia,jb}$ is

$$V^t_{ia,jb}(r_{ia,jb}) = \begin{cases} (13\pi/192)\sigma_t^3, & r_{ia,jb} < \sigma_t \\ \dfrac{\pi\sigma_t^4}{12 r_{ia,jb}}\left(\dfrac{r_{ia,jb}}{\sigma_t} - \dfrac{3}{2}\right)^2\left[\left(\dfrac{r_{ia,jb}}{\sigma_t} + \dfrac{3}{2}\right)^2 - 3\right], & \sigma_t \le r_{ia,jb} \le 3\sigma_t/2 \\ 0, & r_{ia,jb} > 3\sigma_t/2 \end{cases} \quad (4)$$

It also cuts the other shaded portion from the spheres of the neighboring sites (=$a \pm 1$, $a \pm 2$, $a \pm 3$, $a \pm 4$); this volume is denoted by V^t_{ia}. Consequently, the local packing ratio Γ^t_{ia} is defined as

$$\Gamma^t_{ia} = \frac{1}{V^t_{cp}}\left[V^t_{ia} + \sum_{b\in i, |b-a|\ge 5} \beta_b V^t_{ia,ib}(r_{ia,ib}) + \sum_{j\ne i}\sum_{b\in j} \beta_b V^t_{ia,jb}(r_{ia,jb})\right] \quad (5)$$

where the first, second, and third terms in the brackets correspond to the contributions from the intramolecular neighboring sites, the other intramolecular sites, and all the hydrophobic sites of the other molecules, respectively. In eq 5, $V^t_{cp} \equiv V^t_{ia,jb}(\sigma_t) \times 12 = (13\pi/16)\sigma_t^3$ is the closest packing volume for the nonbonded identical spheres of radius $\sigma_t/2$, and β_b is a factor to avoid overestimating the net volume occupied by molecule *j* (e.g., the simple summation of $V^t_{ia,jb}$ over site *b* on molecule *j* causes overestimation of the volume of the overlapping space between the spherical shell of site *a* on molecule *i* and a chain of the spheres on molecule *j*). The distribution parameter $\alpha_{ia,jb}$ is given as a function of the local packing ratio around sites *a* and *b* of interest, $\Gamma^t_{ia,jb}$:

$$\alpha_{ia,jb} = 0.5 + 0.5\tanh\left[\frac{\Gamma^t_{ia,jb} - 0.5}{0.135}\right] \quad (6a)$$

$$\Gamma^t_{ia,jb} = \max(\Gamma^t_{ia}, \Gamma^t_{jb}) - V^t_{ia,jb}(r_{ia,jb})/V^t_{cp} \quad (6b)$$

In the present study, V^t_{ia} and β_b were chosen as the constant values depending on the hydrophobic sites of the surfactant, the all-trans conformation of which was assumed for the sake of convenience. The values of parameters V^t_{ia} and β_b are listed in Table 2, where the hydrophobic sites are numbered 1, ···, 10 from the t next to h^+ to the end t. It should be noted that the values of V^t_{ia} and β_b in Table 2 are slightly different from those in Table 3 of ref 19, because of the difference in definition of V^t_{ia}.

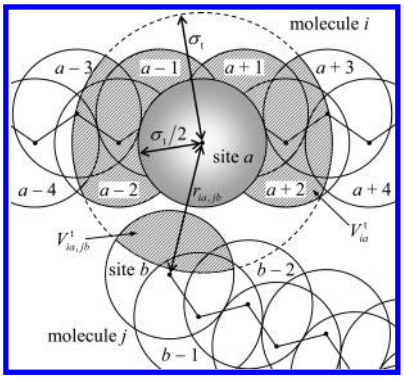

Figure 2. Illustration of hydrophobic chains of two molecules. The spherical shell of inner radius $\sigma_t/2$ and outer radius σ_t around site *a* on molecule *i* cuts out from the sphere of site *b* on molecule *j*, the shaded portion, whose volume is indicated by $V^t_{ia,jb}$. The other shaded portion is cut out from the spheres of the neighboring sites (=$a \pm 1$, $a \pm 2$, $a \pm 3$, $a \pm 4$); this volume is denoted by V^t_{ia}.

Table 2. Parameters of Eqs 5 and 9 for $t_{10}h^+$ Surfactant

	V^t_{ia}/V^t_{cp}	V^h_i/V^h_{cp}	β_b
h^+		0.093	
t1	0.54		0.58
t2	0.48		0.56
t3, ···, t7	0.44		0.53
t8	0.42		0.53
t9	0.33		0.59
t10	0.22		0.75

2.1.2. Present Model (ISM-3). Solute transfer across the interface between two immiscible liquids is accompanied by the free energy change resulting from the difference of the solvation states; therefore, the force perpendicular to the liquid−liquid interface acts on the solute at the interface.[24,25] Likewise, when the surfactants assemble to form an aggregate in water, their charged headgroups situated at the interface between the hydrocarbon core and water feel such forces, which are neglected in the ISM-2. In the present model (ISM-3), these forces, $\mathbf{f}_h$, were modeled as a pseudo-single-body force depending on the local density of hydrocarbon sites around a charged headgroup and were incorporated into the ISM-2 mentioned above.

The force $\mathbf{f}_h$ was represented as a function of the local packing ratio of the hydrophobic sites around the hydrophilic site h^+ on molecule *i*, Γ^h_i

$$\mathbf{f}_h = 0.5\, f_0[\cos\{2\pi(\Gamma^h_i - 0.5)\} + 1]\cdot\frac{\mathbf{r}^h_i - \mathbf{r}^{t2}_i}{|\mathbf{r}^h_i - \mathbf{r}^{t2}_i|} \quad (7)$$

where $\mathbf{r}^h_i$ and $\mathbf{r}^{t2}_i$ are the positions of h^+ and t2 sites, respectively, and $f_0 = 4.5 \times 10^{-10}$ N is the maximum force

derived from the theory of Ulstrup and Kharkats[24] with the relative permittivity of liquid alkane $\epsilon_r^o = 1.9$. The definition of Γ_i^h is similar to that of Γ_{ia}^t described in section 2.1.1. We regarded the hydrophilic site h^+ as a sphere of radius $\sigma_h/2 = 0.285$ nm and then calculated the portion that the spherical shell of inner radius $\sigma_h/2$ and outer radius $r_o \equiv (\sigma_h + \sigma_t)/2$ around the site h^+ cuts out from the spheres of the hydrophobic sites. The volume of the portion that the spherical shell around the site h^+ on molecule i cuts out from the sphere of hydrophobic site b on molecule j, $V_{i,jb}^h$, is

$$V_{i,jb}^h(r_{i,jb}^h) = \begin{cases} (\pi/192)(16 - 3\sigma_t/r_o)\sigma_t^3, & r_{i,jb}^h < r_o \\ \dfrac{\pi\sigma_t^4}{12 r_{i,jb}^h}\left[\dfrac{r_{i,jb}^h}{\sigma_t} - \left(\dfrac{r_o}{\sigma_t} + \dfrac{1}{2}\right)\right]^2\left[\left\{\dfrac{r_{i,jb}^h}{\sigma_t} + \left(\dfrac{r_o}{\sigma_t} + \dfrac{1}{2}\right)\right\}^2 - 4\left(\dfrac{r_o}{\sigma_t} + \dfrac{1}{2}\right)^2 + 6\dfrac{r_o}{\sigma_t}\right], & r_o \le r_{i,jb}^h \le r_o + \sigma_t/2 \\ 0, & r_{i,jb}^h > r_o + \sigma_t/2 \end{cases} \quad (8)$$

Note that eq 8 is identical to eq 4 when $r_o = \sigma_t$ (i.e., $\sigma_h = \sigma_t$). The volume of the portion cut out from the spheres of four neighboring hydrophobic sites (=t1, t2, t3, t4) is denoted by V_i^h. The local packing ratio Γ_i^h is then defined as

$$\Gamma_i^h = \frac{1}{V_{cp}^h - V_i^h}\left[\sum_{b\in i, b\ge t5}\beta_b V_{i,ib}^h(r_{i,ib}^h) + \sum_{j\ne i}\sum_{b\in j}\beta_b V_{i,jb}^h(r_{i,jb}^h)\right] \quad (9)$$

where β_b is the same parameter as in eq 5 and Table 2; $V_{cp}^h \equiv V_{i,jb}^h(r_o) \times 24 = (\pi/8)(16 - 3\sigma_t/r_o)\sigma_t^3$ is an approximation of the closest packing volume for the spheres of radius $\sigma_t/2$ around the sphere of radius $\sigma_h/2$. In the right-hand side of eq 9, V_i^h does not appear in the brackets [···] but does in the denominator to normalize Γ_i^h, because it should never contribute to the force of eq 7 acting on the site h^+ of the surfactant molecule. One should compare eq 9 of Γ_i^h with eq 5 of Γ_{ia}^t, where V_{ia}^t differently appears in the right-hand side to contribute to the interaction force of eq 3a between the hydrophobic sites. Like V_{ia}^t, V_i^h was chosen as the constant value given in Table 2, with the all-trans conformation of the surfactant being assumed.

Table 3. Simulation Systems

system	no. of solutes $t_{10}h^+$	no. of solutes Cl^-	side length L (nm)	concn C_{surf} (M)	initial configuration of surfactants	model
A.1	30	30	7.927	0.1	micelle	ISM-2
A.2	30	30	7.927	0.1	micelle	ISM-3
B.1	343	343	17.86	0.1	monomers	ISM-2
B.2	343	343	17.86	0.1	monomers	ISM-3

2.2. Simulation Details. The systems simulated are summarized in Table 3: (A) a single micelle composed of 30 $t_{10}h^+Cl^-$ surfactants in water at $C_{surf} = 0.1$ M and (B) 343 $t_{10}h^+Cl^-$ surfactants uniformly dispersed in water at $C_{surf} = 0.1$ M. Both the ISM-2 and the ISM-3 were employed in systems A and B to clarify how much the ISM-3 improves the representation of the surfactant solutions. The surfactant concentration of $C_{surf} = 0.1$ M employed in the present study is higher than the critical micelle concentration (cmc) of C_{10}TAC in ambient water, 0.05−0.065 M.[26,27] A cubic box with 3D periodicity was employed, which included the finite number of the solutes and had the side length L as listed in Table 3. The equations of motion for all the interaction sites were integrated by the leapfrog algorithm with the time step of $\Delta t = 0.005$ ps. The bond lengths and the bond angles of the $t_{10}h^+$ surfactant were fixed by the SHAKE method.[15] The temperature of the systems was kept at $T = 300$ K, using the Nosé−Hoover thermostat[15] with a time constant of $\tau_T = 1$ ps. The Coulomb contributions of eq 1 to the PMF were handled by the Ewald summation,[15] while the rest of the contributions were considered only within the range of the computed PMFs (i.e., $r \le 0.8$ or 1.2 nm). In eqs 4−6, 8, and 9, the local packing ratios, Γ_{ia}^t and Γ_i^h, were calculated at every time step. During the simulations, the configuration was stored every 0.1 ps for the subsequent analysis.

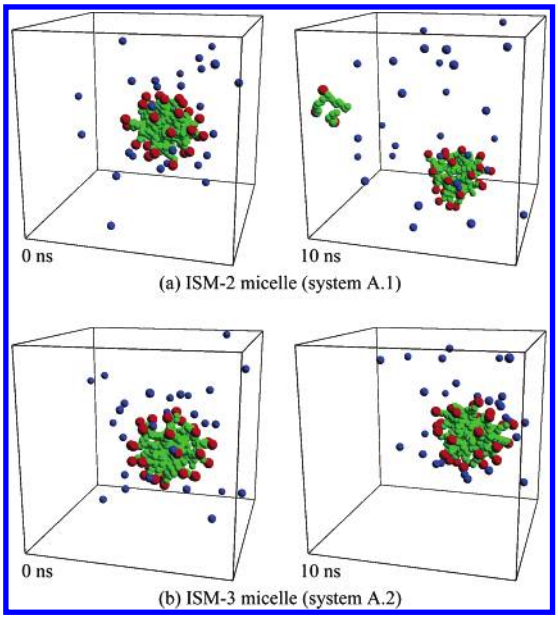

Figure 3. Snapshots of a micelle of 30 $t_{10}h^+Cl^-$ surfactants in water at $C_{surf} = 0.1$ M (system A) at time $t = 0$ and 10 ns: (a) the ISM-2 and (b) the ISM-3. Green, red, and blue spheres denote t, h^+, and Cl^-, respectively. The simulation cell is depicted by the lines.

2.2.1. Single Micelle in Water (System A). A single micelle initially composed of 30 $t_{10}h^+Cl^-$ surfactants in water was simulated using the ISM-2 (system A.1) or the ISM-3 (system A.2). It is noted that the average size of the aggregates, N_{av}, for C_{10}TAC is estimated as $N_{av} = 30$, according to an extrapolation of the experimental results for C_nTAC: $N_{av} = 44$, 62, and 84 for $n = 12$,[28] 14,[29] and 16,[30] respectively. The initial configuration of a micelle was prepared following section 2.4.2 of ref 18, where the time was set at $t = 0$ (see Figure 3), and the system was allowed to evolve over 10 ns.

2.2.2. Surfactant Self-Assembly in Water (System B). An aqueous solution of 343 $t_{10}h^+Cl^-$ surfactants at $C_{surf} = 0.1$ M was simulated using the ISM-2 (system B.1) or the ISM-3 (system B.2). The number and the concentration of the

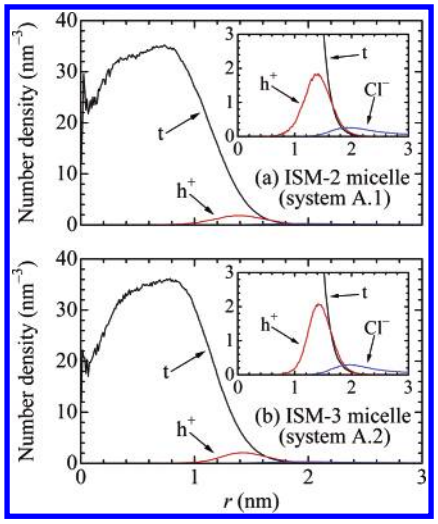

Figure 4. Number densities of t, h^+, and Cl^- for a micelle of 30 $t_{10}h^+Cl^-$ surfactants in water (system A), as a function of the distance from the center of mass of the micelle, *r*. (a) the ISM-2 and (b) the ISM-3. Each density is the result averaged over 20 000 configurations during the last 2 ns of the 10-ns simulation. The inset focuses on the densities of the charged sites.

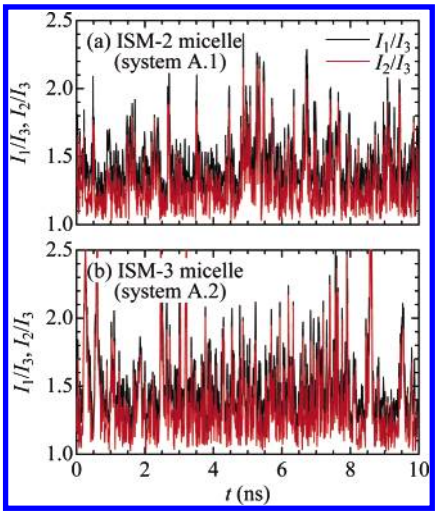

Figure 5. Values of I_1/I_3 (black lines) and I_2/I_3 (red lines) for a micelle of 30 $t_{10}h^+Cl^-$ surfactants in water (system A), as a function of time *t*. (a) the ISM-2 and (b) the ISM-3. The principal moments of inertia of the micelle are represented by I_1, I_2, and I_3, where $I_1 \geq I_2 \geq I_3$. Each plot is the result averaged over 2 ps.

surfactants employed seem to be sufficient for the simulation of the surfactant self-assembly, compared with the average size of the aggregates ($N_{av} = 30$) and the cmc (0.05−0.065 M), respectively. The initial configuration of the surfactants was prepared as follows: (i) the center of mass of a $t_{10}h^+$ surfactant in all-trans conformation was placed at one of the $7 \times 7 \times 7$ lattice points, and the surfactant was then randomly rotated around the lattice point; (ii) likewise, the rest of the surfactants were positioned at the lattice points; and (iii) the Cl^- counterions were placed at random positions such that they never overlapped with each other and the surfactants. Starting from this configuration where the time was set at $t = 0$ (Figure 6a), the system was allowed to evolve over 25 ns.

3. Results and Discussion

In the following two subsections, we investigate the single preformed micelles of 30 surfactants in water (system A) and the self-assembling of surfactants in water (system B) using MD simulations with the ISM-2 and the ISM-3.

3.1. Single Micelle in Water. Figure 3 displays the snapshots of the micelles of 30 $t_{10}h^+Cl^-$ surfactants simulated with the ISM-2 (system A.1) and the ISM-3 (system A.2). For both the models, several surfactants repeatedly dissociated from and associated with the micelle during the 10-ns simulations. At $t = 10$ ns, the ISM-2 and the ISM-3 micelles were composed of 27 and 30 surfactants, respectively; hereafter, a surfactant is considered to belong to the aggregate when the minimum site-to-site separation between the tail of the surfactant and those of the surfactants in the aggregate is less than 0.48 nm, at which the Me−Me PMF equals zero as in Figure 1. Judging from similar snapshots of the ISM-2 and the ISM-3 micelles, the force on the h^+ sites represented by eq 7 seems to have no significant influence on the behavior of single preformed micelles.

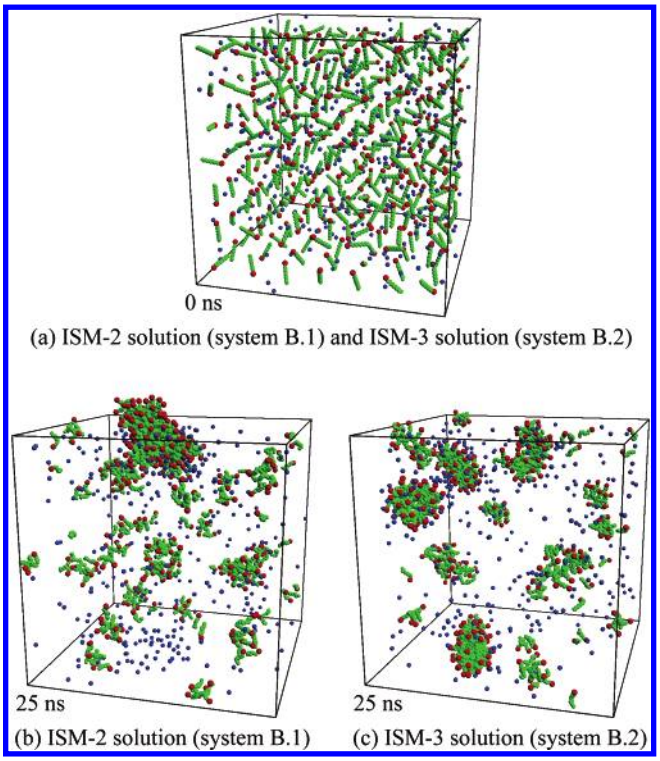

Figure 6. Snapshots of 343 $t_{10}h^+Cl^-$ surfactants in water at $C_{surf} = 0.1$ M (system B): (a) the initial configuration of the ISM-2 and the ISM-3 solutions; (b) the final configuration of the ISM-2 solution; and (c) the final configuration of the ISM-3 solution. Green, red, and blue spheres denote t, h^+, and Cl^-, respectively. The simulation cell is depicted by the lines.

3.1.1. Internal Structure. To investigate the internal structure of the micelle, the number densities of t sites, h^+ sites, and Cl^- counterions were calculated as a function of the distance from the center of mass of the micelle, *r*, using the configurations for $t = 8-10$ ns. Figure 4 exhibits the obtained density profiles. For the ISM-2 micelle, the t sites form a hydrocarbon interior of the micelle at $r \leq 2.0$ nm,

while the h^+ sites exist at the surface of the hydrocarbon core, as in Figure 4a. The Cl^- counterions are located outside of the micelle and favorably reside near the h^+ sites. These profiles coincide with those of the atomistic model MD study, where a micelle of 30 C_{10}TAC surfactants was simulated in 2166 water molecules at $C_{surf} = 0.67$ M for 0.215 ns.[31] Although the density profiles for the ISM-3 micelle are almost the same as those for the ISM-2 micelle, the profile of the h^+ sites for the ISM-3 micelle has a somewhat higher peak at $r \approx 1.4$ nm and a smaller foothill at $t < 1.4$ nm (see the insets of Figure 4). This is because the h^+ sites of the surfactants in the ISM-3 micelle are pushed out of the hydrocarbon interior by the forces of eq 7 depending on the hydrocarbon densities around them.

3.1.2. Shape and Stability. The principal moments of inertia of the micelle, I_1, I_2, and I_3 ($I_1 \geq I_2 \geq I_3$), were calculated to obtain detailed information on the shape and the stability of the micelle. Figure 5 shows the values of I_1/I_3 and I_2/I_3 as a function of time t, where each plot is the result averaged over 2 ps. The values of I_1/I_3 and I_2/I_3 for the ISM-2 and the ISM-3 micelles are larger than unity, indicating that both the micelles have an ellipsoidal shape. The sharp and high peaks of I_1/I_3 and I_2/I_3 result from the dissociation/association of some surfactants from/with the micelle. The values of I_1/I_3 and I_2/I_3 for the ISM-3 micelle fluctuate a bit more significantly than those for the ISM-2 micelle, suggesting that the ISM-3 micelle is slightly less stable than the ISM-2 micelle.

3.1.3. Comparison between ISM-2 and ISM-3. In the previous study,[19] we demonstrated that the ISM-2 successfully represents the preformed micelle of surfactants in water, by comparison with the results of the atomistic model MD study[31] and the NMR study.[32] As seen in Figures 3−5, the behaviors of the ISM-2 and the ISM-3 micelles closely resemble each other, except that there are slight differences in the density profile of the h^+ sites and the values of I_1/I_3 and I_2/I_3. This indicates that the corrected treatment of the h^+ sites in the ISM-3 hardly influences the representation of the single preformed micelle of $N = 30$, which is the average size of the aggregates for C_{10}TAC. Nonetheless, this correction in the ISM-3 significantly improves the representation of surfactant self-assembling, as will be demonstrated in section 3.2.

3.2. Surfactant Self-Assembly in Water. We have ascertained that the ISM-3 can plausibly represent the surfactant micelle of the proper size, as mentioned in section 3.1. Next, we consider the aqueous solution of 343 $t_{10}h^+Cl^-$ surfactants simulated using the ISM-2 (system B.1) and the ISM-3 (system B.2).

Figure 6 displays the snapshots of the aqueous surfactant solutions for the ISM-2 and the ISM-3, where the $t_{10}h^+$ surfactants and the Cl^- counterions at $t = 0$ are completely disaggregated, as expected from the procedure explained in section 2.2.2. At $t = 25$ ns, the surfactants in the ISM-2 solution spontaneously assembled to form a large aggregate of $N = 117$, and the other surfactants existed as monomers or aggregates of $N < 10$, as in Figure 6b. In Figure 6c for the ISM-3 solution, on the other hand, the surfactants formed several aggregates of different sizes,

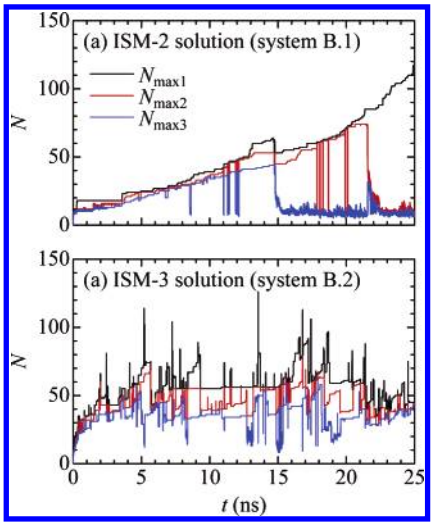

Figure 7. Three maximum sizes N_{max1} (black lines), N_{max2} (red lines), and N_{max3} (blue lines) of surfactant aggregates in $C_{surf} = 0.1$ M solution of 343 $t_{10}h^+Cl^-$ surfactants (system B), as a function of time t: (a) the ISM-2 and (b) the ISM-3.

where the sizes of the three largest aggregates were 46, 44, and 43 at $t = 25$ ns.

3.2.1. Growth Process of Aggregates. To investigate the growth process of the surfactant aggregates, we calculated three maximum sizes of the aggregates, N_{max1}, N_{max2}, and N_{max3}, at every configuration stored during the 25-ns simulation. Figure 7 shows the resultant values of N_{max1}, N_{max2}, and N_{max3} as a function of time t. As seen in Figure 7a, these maximum sizes of the aggregates in the ISM-2 solution gradually increase until $t \leq 14.7$ ns, and then the largest aggregate of $N_{max1} = 63$ breaks apart into monomers and small aggregates. At $t = 21.5$ ns, the second largest aggregate of $N_{max2} = 74$ falls apart. Thereafter, only one large aggregate continues to grow until $t = 25$ ns, as also seen in Figure 6b. For the ISM-3 solution, the values of N_{max1}, N_{max2}, and N_{max3} greatly fluctuate at $t = 2-25$ ns as seen in Figure 7b. The sharp and high peaks of N_{max1}, N_{max2}, and N_{max3} correspond to the temporary association between surfactant aggregates. The continuous fluctuations of N_{max1}, N_{max2}, and N_{max3} in Figure 7b indicate that the growth and the breakup of the surfactant aggregates repeatedly occur in the ISM-3 solution. Thus, the growth process of the surfactant aggregates in the ISM-3 solution is quite different from that in the ISM-2 solution shown in Figure 7a; the latter is considered to be an artifact resulting from the rude treatment of the h^+ sites at the interface between the hydrocarbon core and the implicit water.

3.2.2. Surroundings of Charged Headgroups. We carefully observed the snapshots of the ISM-2 solution to find that the h^+ sites of the ISM-2 surfactants intruded into the hydrocarbon interiors of the large aggregates, whereas the Cl^- counterions never existed there. The former result is implausible because the charged headgroups should exist in water more favorably than in the hydrocarbon interior. To clarify the difference in the surroundings of the h^+ sites between the ISM-2 and the ISM-3 solutions, we counted the number of the t sites in the coordination shell around each h^+ site, $n_{h\to t}$, and then calculated the probability distribution

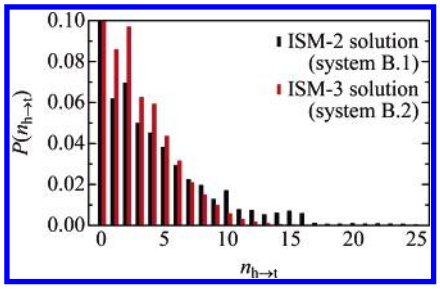

Figure 8. Probability distributions of the h^+ sites with the coordination number $n_{h\to t}$ of the t sites in the shell around each h^+ site, $P(n_{h\to t})$, in the ISM-2 solution (black bars) and the ISM-3 solution (red bars). The value of $P(n_{h\to t})$ at $n_{h\to t} = 0$ and the average coordination number respectively equal to $P(0) = 0.59$ and $\bar{n}_{h\to t} = 2.18$ for the ISM-2 and $P(0) = 0.56$ and $\bar{n}_{h\to t} = 1.61$ for the ISM-3. Each $n_{h\to t}$ includes only the intermolecular contributions. Each distribution is the result averaged over 50 000 configurations during the last 5 ns of the 25-ns simulation.

of the h^+ sites with $n_{h\to t}$, $P(n_{h\to t})$. Here, each $n_{h\to t}$ includes only the intermolecular sites, and the coordination shell was defined as the region of $r_{h\to t} \leq 6.4$ nm, at which the PMF for the Me−TMA^+ pair exhibits the first maximum between two minima as in Figure 1.

The resultant probability distributions are shown in Figure 8, where the probabilities of $n_{h\to t} > 0$ are highlighted and those of $n_{h\to t} = 0$ are 0.59 and 0.56 for the ISM-2 and the ISM-3 solutions, respectively. The probabilities of $n_{h\to t} = 1-6$ for the ISM-2 solution are lower than those for the ISM-3 solution, while the probabilities of $n_{h\to t} \geq 7$ are higher. The average coordination numbers were also calculated and found to be $\bar{n}_{h\to t} = 2.18$ and 1.61 for the ISM-2 and the ISM-3 solutions, respectively. These results suggest that the h^+ sites of the ISM-2 surfactants easily exist in the hydrophobic environment compared with those of the ISM-3 surfactants. In general, the size of an aggregate of ionic surfactants in water is determined by a balance between two interactions: (i) the solvent-induced hydrophobic attraction among the hydrocarbon chains and (ii) the electrostatic repulsion among the charged headgroups, which are located at the interface between the resultant hydrocarbon core and water. The former causes the surfactant aggregation, while the latter limits it. In the ISM-2 solution, the h^+ sites often intruded into the hydrocarbon interiors, which leads to weakening of the electrostatic repulsion among the h^+ sites. This is a reason why the aggregates of the ISM-2 surfactants become much larger than those of the ISM-3 surfactants, as shown in Figures 6b, 7a, and 9a.

By contrast, the behaviors of the ISM-2 and the ISM-3 preformed micelles in system A are fairly similar to each other, as mentioned in section 3.1. According to eqs 7−9, the revision in the ISM-3 has a noticeable influence on the behavior of the surfactant only when its h^+ site is contiguous to the t sites other than its neighboring t sites. Such a situation infrequently arose in system A, because most of the surfactants in the preformed micelle stably existed as an aggregate with the h^+ sites pointing outward and the hydrophobic tails of the t sites pointing inward during the simulation. Thus, the simulation of the preformed micelle

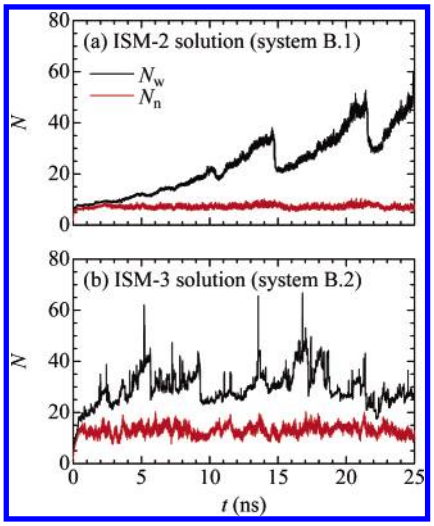

Figure 9. Weight average size N_w (black lines) and number average size N_n (red lines) of the surfactant aggregates in $C_{surf} = 0.1$ M solution of 343 $t_{10}h^+Cl^-$ surfactants (system B), as a function of time t: (a) the ISM-2 and (b) the ISM-3.

of the proper size is inappropriate for examination into how the revision in the ISM-3 impacts on the surfactant behavior.

It is worth noting that the PMFs for interactions of h^+ with the sites (h^+, t, and Cl^-) used in our ISMs are based on a tetramethylammonium cation [$(CH_3)_4N^+$] instead of a trimethylammonium cation [$(CH_3)_3N^+$-]. In this strict sense, one should think that our h^+ site represents a headgroup plus its bonding methylene group, [$(CH_3)_3N^+$-CH_2-], and our $t_{10}h^+Cl^-$ surfactant corresponds to C_{11}TAC rather than C_{10}TAC, which leads to the slightly different values of N_{av} and cmc. However, the conclusions drawn from the present simulations are unaffected.

3.2.3. Size of Aggregates. Figure 9 shows the number average size and the weight average size of the aggregates, N_n and N_w, as a function of time t, which are respectively defined as

$$N_n = \frac{\sum_{N>1} k_N N}{\sum_{N>1} k_N} \tag{10a}$$

$$N_w = \frac{\sum_{N>1} k_N N^2}{\sum_{N>1} k_N N} \tag{10b}$$

where k_N is the number of the aggregates of size N.[33,34] It is worth noting that the light, neutron, and X-ray scattering measurements, which are the popular methods to estimate the average size of surfactant aggregates, give the weight average size of the aggregates, N_w. The average size of the aggregates for C_{10}TAC, $N_{av} = 30$, corresponds to N_w because it is an estimate using an extrapolation of the experimental results obtained by the light scattering[28,29] and the X-ray scattering.[30] As seen in Figure 9a, N_n in the ISM-2 solution is almost constant around 7, while N_w continuously increases during the 25-ns simulation, except for the sharp drops at t

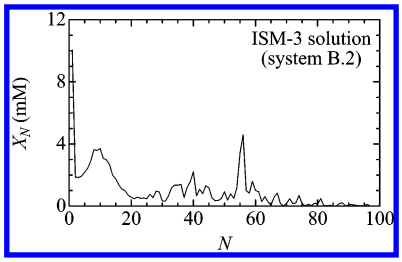

Figure 10. Size distribution of surfactant aggregates in C_{surf} = 0.1 M ISM-3 solution of 343 $t_{10}h^+Cl^-$ surfactants (system B.2). The average concentration of the surfactants in aggregates of size N is denoted by X_N. Each plot is the result averaged over 20 000 configurations taken every 1 ps during the last 20 ns of the 25-ns simulation.

= 14.7 and 21.5 ns corresponding to the breakups of the large aggregates shown in Figure 7a. Finally, N_w exceeds the average size of the aggregates $N_{av} = 30$ for C_{10}TAC and reaches 53.4 at $t = 25$ ns. For the ISM-3 solution, both N_n and N_w seem to converge and fluctuate around constant values at least at $t > 5$ ns as in Figure 9b. The averages of N_n and N_w over $t = 5-25$ ns are 13.3 and 30.6, respectively; the latter value for N_w agrees very well with the experimental estimate of $N_{av} = 30$.

For the ISM-3 solution, the aggregate size distribution was calculated using the configurations for $t = 5-25$ ns, which are considered to be equilibrated judging from the variations of the maximum sizes of the aggregates (Figure 7b) and of the average sizes (Figure 9b). Figure 10 shows the resultant size distribution of the aggregates, where X_N denotes the average concentration of the surfactants in the aggregates of size N. The aggregates in the ISM-3 solution exhibit several favorable sizes of $N < 100$, and the maximum peak is observed at $N = 56$. However, the size distribution in Figure 10 is not smooth enough because of the lack of the sufficient samplings. Although we performed the ISM-3 simulations using the single CPU computers in the present study, the use of the massive parallel computers may enable us to carry out the long-time simulations of the large-scale systems for the sufficient samplings. This will be our future study.

4. Conclusions

We have recently proposed a series of the ISMs for the simulation of cationic surfactants in water, where no water molecules of solvent are explicitly treated and their effects are incorporated using the solvent-averaged interactions, namely PMFs.[18,19] In our previous study, the ISM was revised to improve the representation of the hydrocarbon interior of the surfactant aggregates: in this revised ISM (ISM-2),[19] the interactions between the hydrophobic sites of the surfactants are varied depending on the hydrocarbon densities around them, while in the original ISM,[18] all the interactions between the surfactant segments are given by the PMFs regardless of their surroundings. In the present study, we have additionally improved the representation of a charged headgroup of the liquid−liquid interface between the hydrocarbon oil and the implicit water, where the free energy change due to the transfer of the charged headgroup across the interface is taken into account. The present model (ISM-3) has been applied to the MD simulations of (i) a single preformed micelle composed of 30 C_{10}TAC cationic surfactants in water and (ii) 343 C_{10}TAC surfactants uniformly dispersed in water, where the corresponding systems were also simulated using the ISM-2 for comparison. The first simulations showed that the ISM-3 as well as the ISM-2 is applicable to the simulation of the preformed micelle of the average aggregate size for C_{10}TAC, judging from the internal structure, the shape, and the stability of the micelle. In the second simulations, the ISM-2 solution gave the strange result that only a few surfactant aggregates became large and the other surfactants remained as monomers or small aggregates; for the ISM-3 solution, on the other hand, the surfactant self-assembling was plausibly represented in the sense that the weight average size of the aggregates agreed very well with the experimental estimate.

The ISM-3 simulation of aqueous surfactant solutions computationally costs far less than the atomistic model simulations do, where the water molecules of the solvent are explicitly treated in addition to the solutes of interest. The other feature of the ISM-3 is that it allows us to change the concentration of the surfactants and the counterions involved without changing the computational cost because of the implicit treatment of the water molecules. In the near future, we will investigate the effects of the surfactant concentration and the salt addition on the surfactant behavior, with the help of these advantages of the ISM-3 simulation.

Acknowledgment. This work was partly supported by the Grants-in-Aid (No. 15206085/16760606) for Scientific Research from the Ministry of Education, Culture, Sports, Science and Technology in Japan.

References

(1) Klein, M. L. *J. Chem. Soc., Faraday Trans.* **1992**, *88*, 1701.

(2) Smit, B. In *Computer Simulation in Chemical Physics*; Allen, M. P., Tildesley, D. J., Eds.; NATO Advanced Study Institute Series C; Kluwer: Dordrecht, The Netherlands, 1993; Vol. 397, Chapter 12.

(3) Pastor, R. W. *Curr. Opin. Struct. Biol.* **1994**, *4*, 486.

(4) Esselink, K.; Hilbers, P. A. J.; Karaborni, S.; Siepmann, J. I.; Smit, B. *Mol. Simul.* **1995**, *14*, 259.

(5) Karaborni, S.; Smit, B. *Curr. Opin. Colloid Interface Sci.* **1996**, *1*, 411.

(6) Larson, R. G. *Curr. Opin. Colloid Interface Sci.* **1997**, *2*, 361.

(7) Jakobsson, E. *Trends Biochem. Sci.* **1997**, *22*, 339.

(8) Bandyopadhyay, S.; Tarek, M.; Klein, M. L. *Curr. Opin. Colloid Interface Sci.* **1998**, *3*, 242.

(9) Shelley, J. C.; Shelley, M. Y. *Curr. Opin. Colloid Interface Sci.* **2000**, *5*, 101.

(10) Feller, S. E. *Curr. Opin. Colloid Interface Sci.* **2000**, *5*, 217.

(11) Forrest, L. R.; Sansom, M. S. P. *Curr. Opin. Struct. Biol.* **2000**, *10*, 174.

(12) Schmid, F. In *Computational Methods in Surface and Colloid Science*; Borówko, M., Ed.; Surfactant Science Series 89; Marcel Dekker: New York, 2000; Chapter 13.

(13) Saiz, L.; Bandyopadhyay, S.; Klein, M. L. *Biosci. Rep.* **2002**, *22*, 151.

(14) Allen, M. P.; Tildesley, D. J. *Computer Simulation of Liquids*; Clarendon Press: Oxford, U.K., 1987.

(15) Frenkel, D.; Smit, B. *Understanding Molecular Simulation: From Algorithms to Applications*, 2nd ed.; Academic Press: San Diego, CA, 2002.

(16) Rapaport, D. C. *The Art of Molecular Dynamics Simulation*, 2nd ed.; Cambridge University Press: Cambridge, U.K., 2004.

(17) Roux, B.; Simonson, T. *Biophys. Chem.* **1999**, *78*, 1.

(18) Shinto, H.; Morisada, S.; Miyahara, M.; Higashitani, K. *Langmuir* **2004**, *20*, 2017.

(19) Morisada, S.; Shinto, H.; Higashitani, K. *J. Phys. Chem. B* **2005**, *109*, 11762.

(20) Lazaridis, T.; Mallik, B.; Chen, Y. *J. Phys. Chem. B* **2005**, *109*, 15098.

(21) (a) Shinto, H.; Morisada, S.; Miyahara, M.; Higashitani, K. *J. Chem. Eng. Jpn.* **2003**, *36*, 57. (b) Shinto, H.; Morisada, S.; Higashitani, K. *J. Chem. Eng. Jpn.* **2004**, *37*, 1345. (c) Shinto, H.; Morisada, S.; Higashitani, K. *J. Chem. Eng. Jpn.* **2005**, *38*, 465.

(22) The Chemical Society of Japan. *Kagaku-binran Kiso-hen II*, 4th ed.; Maruzen: Tokyo, Japan, 1993.

(23) Ryckaert, J.-P.; Bellemans, A. *Faraday Discuss. Chem. Soc.* **1978**, *66*, 95.

(24) Ulstrup, J.; Kharkats, Y. I. *Russ. Electrochem.* **1993**, *29*, 386.

(25) Schweighofer, K.; Benjamin, I. *J. Phys. Chem. A* **1999**, *103*, 10274.

(26) Bacaloglu, R.; Blaskó, A.; Bunton, C. A.; Cerichelli, G.; Ortega, F. *J. Phys. Chem.* **1990**, *94*, 5062.

(27) Klevens, H. B. *J. Am. Oil Chem. Soc.* **1953**, *30*, 74.

(28) Ozeki, S.; Ikeda, S. *Bull. Chem. Soc. Jpn.* **1981**, *54*, 552.

(29) Imae, T.; Ikeda, S. *J. Phys. Chem.* **1986**, *90*, 5216.

(30) Reiss-Husson, F.; Luzzati, V. *J. Phys. Chem.* **1964**, *68*, 3504.

(31) Böcker, J.; Brickmann, J.; Bopp, P. *J. Phys. Chem.* **1994**, *98*, 712.

(32) Stilbs, P.; Walderhaug, H.; Lindman, B. *J. Phys. Chem.* **1983**, *87*, 4762.

(33) Mukerjee, P. *J. Phys. Chem.* **1972**, *76*, 565.

(34) Nagarajan, R. *Langmuir* **1994**, *10*, 2028.

CT600311T